

The Effect of Atomic-Scale Roughness on the Adhesion of Nanoscale Asperities: A Combined Simulation and Experimental Investigation

Tevis D. B. Jacobs · Kathleen E. Ryan · Pamela L. Keating ·
David S. Grierson · Joel A. Lefever · Kevin T. Turner ·
Judith A. Harrison · Robert W. Carpick

Received: 5 October 2012 / Accepted: 26 December 2012 / Published online: 10 February 2013
© Springer Science+Business Media New York 2013

Abstract The effect of atomic-scale roughness on adhesion between carbon-based materials is examined by both simulations and experimental techniques. Nanoscale asperities composed of either diamond-like carbon or ultrananocrystalline diamond are brought into contact and then separated from diamond surfaces using both molecular dynamics simulations and in situ transmission electron microscope (TEM)-based nanoindentation. Both techniques allow for characterization of the roughness of the sharp nanoasperities immediately before and after contact down to the subnanometer scale. The root mean square roughness for the simulated tips spanned 0.03 nm (atomic corrugation) to 0.12 nm; for the experimental tips, the range was 0.18–1.58 nm. Over the tested range of roughness, the measured work of adhesion was found to decrease by more than an order of magnitude as the roughness increased. The dependence of adhesion upon

roughness was accurately described using a simple analytical model. This combination of simulation and experimental methodologies allows for an exploration of an unprecedented range of tip sizes and length scales for roughness, while also verifying consistency of the results between the techniques. Collectively, these results demonstrate the high sensitivity of adhesion to interfacial roughness down to the atomic limit. Furthermore, they indicate that care must be taken when attempting to extract work of adhesion values from experimental measurements of adhesion forces.

Keywords Adhesion · Surface roughness · In situ TEM · Molecular dynamics simulation · Nanotribology · AFM · Diamond · Diamond-like carbon

Electronic supplementary material The online version of this article (doi:10.1007/s11249-012-0097-3) contains supplementary material, which is available to authorized users.

T. D. B. Jacobs · J. A. Lefever
Department of Materials Science & Engineering,
University of Pennsylvania, 3231 Walnut St.,
Philadelphia, PA 19104, USA
e-mail: tevis@seas.upenn.edu

K. E. Ryan · P. L. Keating · J. A. Harrison
Department of Chemistry, United States Naval Academy,
5122 Holloway Road, Annapolis, MD 21402, USA

D. S. Grierson
systeMECH, LLC, Madison, WI 53705, USA

K. T. Turner · R. W. Carpick (✉)
Department of Mechanical Engineering & Applied Mechanics,
University of Pennsylvania, 220 S. 33rd St., Philadelphia,
PA 19104, USA
e-mail: carpick@seas.upenn.edu

1 Introduction and Motivation

1.1 Work of Adhesion and its Measurement

The work of adhesion, W_{adh} , between two surfaces is an important property of an interface that governs adhesion forces and contact stresses, and can strongly influence friction and wear between two bodies [1]. For a given pair of materials, continuum mechanics models [2–4] assume a single, constant value of W_{adh} [J/m²], which represents the energy per unit area to separate two perfectly flat surfaces from equilibrium contact to infinite separation. Knowledge of W_{adh} is important for research and applications in many areas, including thin-film coatings [5], biological and biomimetic adhesion [6], composites [7], and micro/nanoelectromechanical systems (MEMS/NEMS) [8]. A common method to characterize the work of adhesion between two surfaces is to use an atomic force microscope (AFM) to measure the force, $F_{\text{pull-off}}$, required to separate a nanoscale

tip of radius, R_{tip} , from a nominally flat sample. Then, single-asperity continuum contact mechanics models (such as Derjaguin–Müller–Toporov (DMT) [2], Johnson–Kendall–Roberts (JKR) [3], or Maugis–Dugdale [4]) can be applied to extract a work of adhesion as [9]:

$$W_{\text{adh,eff}} = \frac{F_{\text{pull-off}}}{\chi\pi R_{\text{tip}}}, \quad (1)$$

where χ is a constant that ranges between 1.5–2 (determined based on properties of the contact pair, as discussed in [4]). Equation 1 assumes small strains, that the materials are homogeneous, isotropic, and linearly elastic, and that the tips are perfectly smooth with a paraboloidal geometry (i.e., a three-dimensional revolution of a parabola). This quantity is designated here as the *effective* work of adhesion, $W_{\text{adh,eff}}$, to distinguish the value measured with a rough tip from $W_{\text{adh,max}}$, the work of adhesion measured with an atomically smooth tip (as discussed later).

1.2 Prior Work on Roughness and its Effect on Adhesion

Previous experimental and theoretical work has demonstrated that pull-off forces are highly sensitive to surface roughness. For example, Fuller and Tabor examined adhesion between rubber spheres with radii from 7 to 53 mm and (nominally flat) roughened stiff surfaces [10]. They found a 90 % drop in the apparent work of adhesion as the average roughness, R_a , of the flat surface increased from 0.12 to 1.4 μm . Separate studies on micromachined surfaces showed a fourfold reduction in adhesion as the root mean square (RMS) roughness (designated R_q) increased from 3 to 10 nm [11] and a tenfold reduction for surfaces where RMS roughness increased from 10 to 40 nm [12]. When adhesion studies were performed using microscale colloidal beads [13, 14] (radii 2–10 μm) or intentionally flattened AFM probes [15] (flattened areas 600–47,000 nm^2) on surfaces of varying roughness, all showed more than an order of magnitude drop in pull-off force with increasing roughness (RMS roughness ranging from approximately 1 to 10 nm in both studies). However, there have been very few experimental investigations into the effect of roughness on contacts where one body is a nanoscale tip, as is the case in tip-based microscopy and manufacturing. In one such study, adhesion tests using AFM probes with tip radii of 200 nm showed a roughly fourfold reduction in adhesion force as the RMS roughness of the surface increased from 5–15 nm, but there was a significant degree of scatter in the data [16].

Numerous models have been constructed that examine the effect of roughness on the adhesion of nominally flat surfaces. Greenwood and Williamson's [17] seminal work on the effect of roughness on the contact between two

non-adhesive half spaces considered a flat surface in contact with one that is rough. The roughness is represented by a set of non-interacting asperities with identical radii and a Gaussian distribution of heights. Hertzian mechanics was then applied to determine the forces and deformations of the resulting multi-asperity contact. A key finding was that, even for small levels of roughness, the true contact area is a small fraction of the apparent area. The adhesion of rough surfaces with an assumed geometry similar to that used by Greenwood and Williamson was later examined by Fuller and Tabor (for the JKR limit of adhesion [10]) and Maugis (for the DMT limit [18]). The results of these models agree qualitatively with experiments. However, describing the rough surface as a number of identical asperities with a Gaussian distribution of asperity heights fails to capture both the multiscale nature of roughness that many real surfaces possess and the significant effect of elastic coupling between asperities. An approach that overcomes these limitations is that of Persson, in which a rough surface is treated as an elastic body with self-affine fractal topography containing roughness on many length scales [19]. However, whether roughness is modeled at one or multiple scales, all models predict a rapid decrease in adhesion force with increasing roughness because the real contact area is reduced.

Recent experimental work indicates that it is not sufficient to consider only the asperities that are in intimate contact (as is done in the models discussed above), especially for stiff materials. DelRio et al. [11] used adhesion experiments on micromachined cantilevers as well as numerical simulations to show that up to 65 % of the total adhesive force arises due to the van der Waals attraction from portions of the surfaces that are *near* to contact, but not *in* contact. Therefore, in another avenue of roughness modeling, the van der Waals attraction is integrated between model interfaces to calculate the total adhesive force between them [15, 20, 21]. These models also predict a precipitous drop in adhesion force with increasing roughness because roughness increases the average separation between the two bodies.

However, all of these models assume that the rough surface is nominally flat. Thus, they are not well suited for understanding the effect of roughness of a highly curved tip such as an asperity with nanometer-scale dimensions. Further, due to the difficulty of characterizing the sub-nanometer topography of sharp tips, there have been very few direct investigations of such situations. Using molecular dynamics (MD) simulations of a larger curved surface ($R_{\text{tip}} = 441 \text{ nm}$), Mulakaluri and Persson applied the self-affine fractal model to show an order of magnitude drop in adhesion as roughness increased from 0.1 to 1.2 nm [22]. Luan and Robbins used atomistic simulations on tips that are closer to AFM dimensions ($R_{\text{tip}} \sim 30 \text{ nm}$) to examine

the effect of surface topography. They demonstrated a factor of 2–4 change in adhesion of amorphous surfaces as compared to bent or cut crystalline surfaces [23]. Finally, a recent MD study using flat surfaces showed that the adhesion of a model diamond nanocomposite (on a diamond counter-surface) decreased fourfold when RMS roughness increased from 1.2 to 1.5 Å [24].

In the present investigation, pull-off tests were performed by both MD simulations and in situ TEM nanoindentation measurements, such that the asperity geometry could be characterized with subnanometer-scale detail. The chosen tip materials are diamond-like carbon (DLC) and ultrananocrystalline diamond (UNCD), both are commonly used as wear-resistant coatings in a variety of applications from AFM tips [25] to hard disk read/write heads [26] to MEMS/NEMS [27]. From the pull-off measurements, an effective value of work of adhesion, $W_{\text{adh,eff}}$, was calculated using Eq. 1, where $F_{\text{pull-off}}$ was measured and R_{tip} was determined by fitting a smooth parabola to the overall shape of the asperity. From this, the dependence of adhesion on surface roughness was determined.

The structure of the present paper is as follows: In Sect. 1 (this section), the literature on roughness and adhesion was surveyed, and it was shown that existing models do not explicitly treat the case where a nanoscale tip itself contains roughness. Therefore, in Sect. 2, calculations are presented for a simple numerical model to uncover basic trends to expect for the adhesion as a function of tip roughness. Section 3 presents adhesion data from MD simulations of nanoscale tips with different degrees of roughness pulling off of atomically flat surfaces, and a method for characterizing the RMS roughness of highly curved tips is described. Section 4 contains results from experimental adhesion tests performed using in situ TEM, in which sharp AFM probes with different degrees of roughness were pulled off of a flat substrate under conditions (i.e., environment, materials, and geometry) similar to those of the simulations. In Sect. 5, the TEM and MD data are fit using a closed-form equation from a previously published model described in Sect. 1; qualitative and quantitative trends are discussed in reference to that model and to the numerical model presented in Sect. 2. Finally, Sect. 6 presents concluding remarks.

2 Predicting Trends Using a Simplified Rigid Model

In the absence of a model from the literature for adhesion of rough, curved tips, a simple numerical model is presented that reproduces the essential trend as a function of roughness. An axisymmetric tip is defined by superposing a paraboloid (for the overall tip shape) and a sine wave (representing the roughness) as follows:

$$z_{\text{tip}}(r) = z_{\text{paraboloid}}(r) + z_{\text{roughness}}(r) = \frac{r^2}{2R_{\text{tip}}} - A \cos\left(\frac{2\pi r}{\lambda}\right), \quad (2)$$

where r and z are polar spatial coordinates, R_{tip} defines the radius of the overall parabolic shape, and A and λ are the amplitude and wavelength of the sine wave, respectively. The resulting tip (Fig. 1) is treated as rigid and is brought into contact with a rigid flat surface.

The force of interaction between the tip and the sample is calculated as an integral of an interaction potential between vertically aligned differential elements of the two bodies. The specific interaction potential used was the Lennard-Jones 3-9 surface potential, as is done in several other contact models such as [28] and [29]. This method (integration of surface interactions) is analogous to the method used by Maugis [4], but the interaction potential used here is considered more realistic than the Dugdale potential used in that work. Thus, the total force acting between the tip and sample is determined by the integration of the interaction potential as follows:

$$F = \int_{\text{Area}} \sigma_{\text{normal}}(z_{\text{sep}}) dA = \int_0^{2\pi} \int_0^{\infty} \sigma_{\text{normal}}(z_{\text{sep}}(r, \theta)) r dr d\theta \\ = \int_0^{\infty} \left\{ \frac{8W_{\text{adh}}}{3z_0} \left[\left(\frac{z_0}{z_{\text{sep}}(r)} \right)^3 - \left(\frac{z_0}{z_{\text{sep}}(r)} \right)^9 \right] \right\} 2\pi r dr, \quad (3)$$

where σ_{normal} is the stress acting between two vertically aligned differential elements of area separated by z_{sep} , and z_0 is the equilibrium separation between flat surfaces. In this case, $z_{\text{sep}} = z_{\text{tip}} + d$, where d is the distance of closest approach between tip and sample.

To extract a force-versus-separation curve for the axisymmetric tip separating from the flat surface, the total force acting between the tip and the surface is determined via numerical integration of Eq. 3 for values of d ranging from equilibrium contact to the separation value at which the interaction force reaches its minimum value. This maximum adhesive force achieved during separation is taken to be $F_{\text{pull-off}}$. The numerical integration is performed using custom scripts written in MATLAB. Values of $W_{\text{adh}} = 0.15 \text{ J/m}^2$, $z_0 = 0.154 \text{ nm}$, and $R_{\text{tip}} = 10 \text{ nm}$ to define the potential were chosen because they are similar to the experimental and simulation values; the exact values are unimportant as the qualitative trends would be similar for other common experimental values. The roughness of the tip is changed by varying the amplitude and the wavelength of $z_{\text{roughness}}$ over the range $0 - R_{\text{tip}}/10$ (i.e., 0–1 nm for $R_{\text{tip}} = 10 \text{ nm}$), and the RMS roughness of the tip is calculated from the profile of $z_{\text{roughness}}$. Once $F_{\text{pull-off}}$ is calculated for each value of RMS roughness, Eq. 1 is used to calculate the effective work of adhesion,

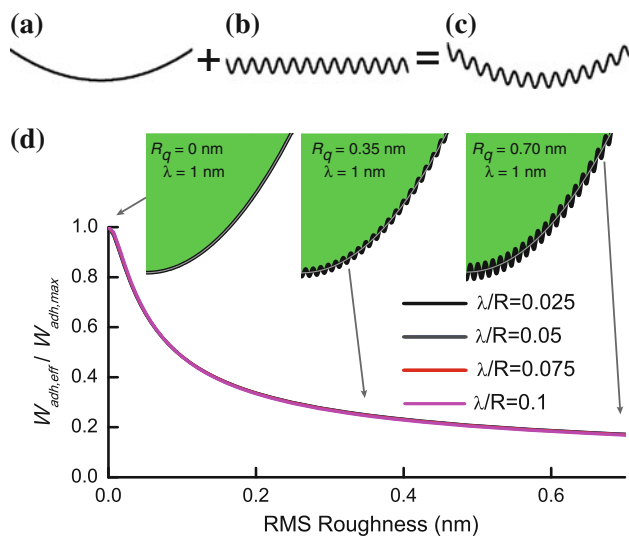


Fig. 1 Using a simple numerical model, a smooth paraboloidal tip (a) has a sinusoidal roughness (b) superimposed on it to create a roughened tip (c). Simulated pull-off force tests as a function of roughness yield values for $F_{pull-off}$ which can be combined with the known overall shape to calculate an effective work of adhesion, $W_{adh,eff}$, according to the DMT model (Eq. 1). This $W_{adh,eff}$ value can be divided by the input $W_{adh,max}$ to determine the deviation due to RMS roughness R_q , as shown in (d) for various values of roughness wavelength λ . Results for all four values of λ overlap, with a maximum deviation of just 2 % at any value of roughness. *Insets* in (d) indicate the roughness as compared to the overall shape (*thin gray lines* show the best-fit parabolic profiles) for three values of roughness. Note that for the tips and data shown in (d), $R_{tip} = 10$ nm and $z_0 = 0.154$ nm

$W_{adh,eff}$. This quantity represents the work of adhesion that would be calculated if the roughness of the tip was ignored, i.e., if only the overall paraboloidal tip shape was considered. In fact, that is how the vast majority of experimental studies calculate the work of adhesion since atomic-scale details of the tip are usually not measurable. In this simple model, the bodies are rigid and therefore have an infinite elastic modulus, corresponding to a Maugis parameter [4] approaching zero (also known as the Bradley limit as discussed by Johnson [30]); thus, $\chi = 2$ in Eq. 1. The numerical accuracy of the simple rigid model has been verified by conducting pull-off simulations of two simple geometries—a flat surface being separated from a flat surface, and a perfectly smooth paraboloid being separated from a flat surface. The separation of two flat surfaces yields a work of adhesion exactly equal to the input value, and the separation of a paraboloid from a flat surface yields a work of adhesion that follows Eq. 1 with $\chi = 2$.

The results of this simplified rigid model are shown in Fig. 1d. The effective work of adhesion is normalized by $W_{adh,max}$ (i.e., the input value for work of adhesion in the interaction potential). This is shown as a function of the RMS roughness R_q , calculated from the sine wave. While

the model and its assumptions are quite simplistic, there are three key implications that provide insights for the measured data discussed in the later sections:

1. The effective work of adhesion decreases significantly and rapidly with increasing roughness. Even with an RMS roughness of just 0.1 nm, the effective work of adhesion is reduced by slightly more than 50 % of its maximum value
2. The results agree qualitatively with findings of the more sophisticated models discussed in Sect. 1. Larger roughness (i.e., larger R_q) increases the average separation between the two surfaces and thus decreases the adhesive stress acting between them. Because the results have been normalized to the maximum (smooth-tip) work of adhesion, these trends are not expected to be material dependent
3. The results show almost no dependence on the wavelength of the roughness, when the wavelength is kept significantly smaller than the tip radius. Over the range shown in Fig. 1d ($0.025 \leq \lambda/R \leq 0.1$), there is only a 2 % change in normalized work of adhesion due to changes in wavelength.

The quantitative reduction of $W_{adh,eff}$ with increasing roughness is sensitive to the chosen value of the equilibrium separation, z_0 ; however, the sharply decreasing trend of $W_{adh,eff}$ as a function of roughness will occur for any reasonable value chosen.

3 Simulated Adhesion Tests using Molecular Dynamics

3.1 Simulation Details

The MD systems were designed to correlate with the experimental systems as closely as possible. Bulk DLC was created by heating diamond to 8,000 K using a Langevin [31] thermostat then quenching to 0 K, and finally heating in 100 K increments of 10 ps each until the final temperature reached 300 K. The bulk DLC material contained 16 % sp^3 -hybridized, 69 % sp^2 -hybridized, 14 % sp -hybridized, and about 1 % over-coordinated carbon. Bulk UNCD was created by placing randomly shaped C(111) and C(001) grains into four-sided columns to form a nanostructured material box. The atoms within 0.2 nm of the edge of each diamond grain were heated to 8,000 K to form amorphous boundaries between grains. The widths of the final UNCD grains were approximately 2–4 nm and with typical grain boundary widths of 0.2 nm, in close agreement with the known structural properties of UNCD [32].

To create axisymmetric paraboloidal asperities, tips were cut from the bulk samples of DLC or UNCD according to the equation:

$$z(r) = \frac{r^2}{2R_{\text{tip}}}, \quad (4)$$

where R_{tip} (the radius of curvature) was set at 2.5 nm and the height of the tip along the z -axis was set at 3.5 nm. The radius of curvature of the tips was selected to be as large as was computationally feasible. After the tips were cut from the bulk sample, the system energy was minimized by equilibrating the tip to 0 K. The tips were then equilibrated to 300 K in 100 K increments. Finally, the tips were terminated with hydrogen by placing them in a box of hydrogen atoms at 300 K and allowing the hydrogen atoms to bond to unsaturated carbon atoms. Equilibrated tips are shown in Fig. 2a–d. These axisymmetric tips were brought into contact with the hydrogen-terminated (111) face of diamond (shown in Fig. 2a). To further analyze the effect of roughness on adhesion, additional tips were created with similar geometry, but intentionally roughened surfaces. To create these rougher tips, the energy of the existing tips was minimized followed by random removal of 25 % of the carbon atoms from the outer 3–5 Å of the tip. The energy of these roughened tips was minimized by a steepest-descent algorithm. The temperature of the tips was then increased in 100-K increments of 5 ps each until the tip

reached 300 K. If carbon atoms with hydrogen termination were removed, the hydrogen was free to rebond in another tip location. After the roughened tips were equilibrated to 300 K, unbonded hydrogen atoms that remained were removed from the simulation. To ensure equilibrium hydrogen termination of the outermost carbon atoms, the tips were placed in a box of atomic hydrogen for 10 ps.

The adhesion simulations were performed using the adaptive intermolecular reactive empirical bond-order potential (AIREBO) [33] as coded into the Large-scale Atomic/Molecular Massively Parallel Simulator (LAMMPS) [34, 35]. The AIREBO potential is based on the second-generation REBO potential designed for carbon- and hydrogen-containing materials [36]. In addition to the covalent bonding terms of the REBO potential, the AIREBO potential includes torsional and intermolecular terms. Simulated systems were first initialized by designating atoms in the outermost layers of both the tip and surface to be held rigid (Fig. 2a–d). Adjacent to the rigid layer, a thermostatted layer of 3–5 Å was created and held at 300 K using the Langevin thermostat. The remaining atoms were free (i.e., without mathematical constraints), and periodic boundary conditions were applied in the plane containing the surface of the substrate (i.e., perpendicular

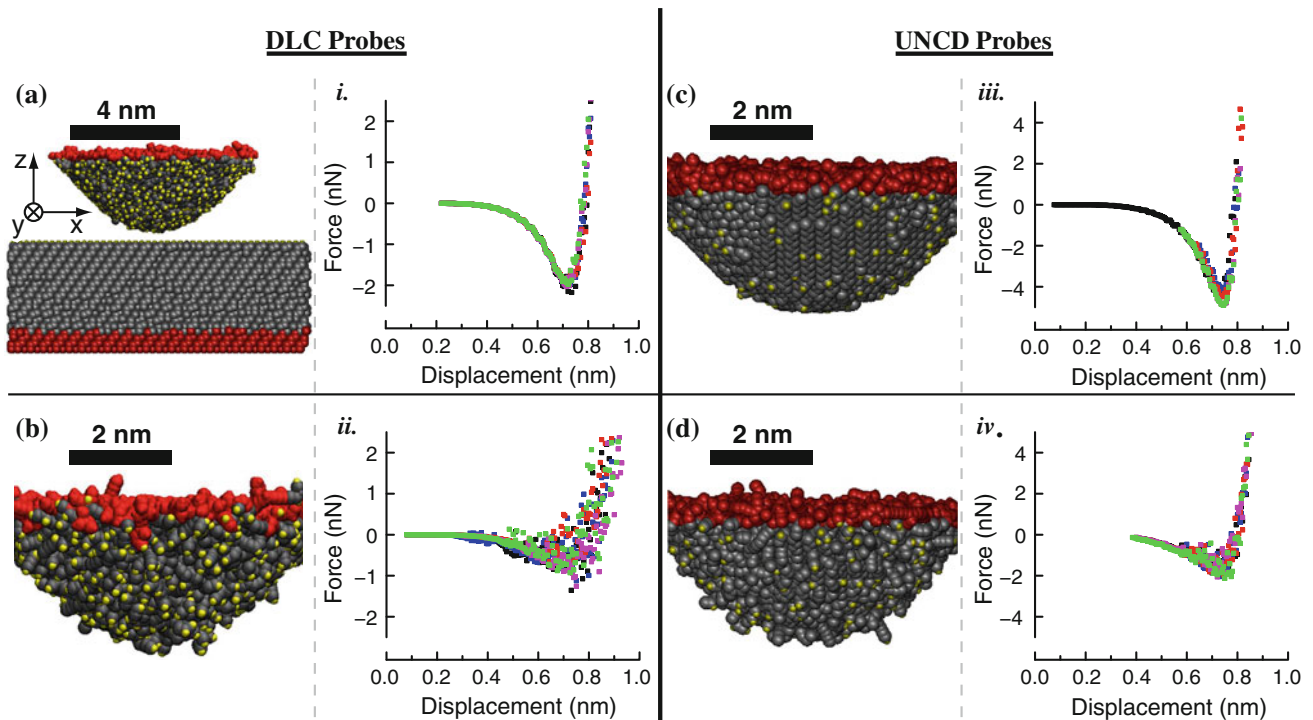


Fig. 2 Simulation tips made from DLC and UNCD (a, c) are shown with carbon atoms colored gray and hydrogen atoms colored yellow; red atoms represent those that are held rigid during simulation. Replicas of these tips were roughened intentionally (b, d). Adhesion tests were performed against a hydrogen-terminated diamond substrate (included in a) to calculate the interaction force as a function of

z -displacement, as shown in (i–iv). Data points from five tests performed with slightly different contact locations are shown overlapped (each with a different color, online) to indicate the degree of scatter in repeated tests. For both materials, the rougher tips demonstrate reduced pull-off forces and larger variability in force curves (Color figure online)

to the indentation direction). Indentation simulations were performed by applying a constant velocity of 0.5 \AA/ps to the rigid layer of the tip in the direction of the surface. Newton's equations of motion were integrated with a time step of 0.25 fs to determine the positions, velocities, and accelerations of each atom at each simulation step. Prior to indentation, the tip was initially placed above the center of the C(111)-H substrate. To account for crystalline alignment effects, multiple impact points were chosen by shifting the tip by one half or one full length of the unit cell of diamond in each lateral direction in a manner similar to [24]. (The unit cell distances are 0.126 and 0.218 nm in the x - and y -directions (Fig. 2a), respectively.)

The atomic contact force on every tip atom due to the surface atoms is calculated at every simulation step. An atomic contact force can be defined as the vector sum of forces exerted on each atom due to interactions with the entire set of atoms of which it is not a member [37]. It is important to note that this atomic contact force shows little connection to the net force on the atom because the forces exerted by all other sample atoms are disregarded. However, the net forces on the individual atoms of either set (tip or sample) summed vectorially give the same result as the vector sum of the atomic contact forces of either set with an overall difference in sign if comparing opposite sets. In other

words, the net force exerted by the tip on the sample is equal and opposite to the net force exerted by the sample on the tip, and these forces can be calculated by summing either net forces or atomic contact forces. Contact forces are more useful than net forces because they can be analyzed in useful ways to elucidate atomic-scale phenomena occurring at the interface between the contacting bodies [37–39].

The atomic contact forces on the tip are summed to yield the total force on the tip. To generate force-versus-distance curves during indentation, the total force on the tip in the indentation (z) direction was averaged every 400 time steps. The displacement at each time step was calculated as the current separation distance between the rigid layers of the tip and the surface minus their initial separation. The pull-off force was identified as the minimum value of force as a function of displacement, as shown in Fig. 2i–iv.

3.2 Characterizing Roughness

For the roughened tips used in the MD simulations, the Cartesian coordinates of every atom in the asperity are known. However, a method for characterizing roughness is needed that can be equally well-applied to the TEM images of real tips, in which only a two-dimensional side-view of the tip is captured. Therefore, a technique was devised for

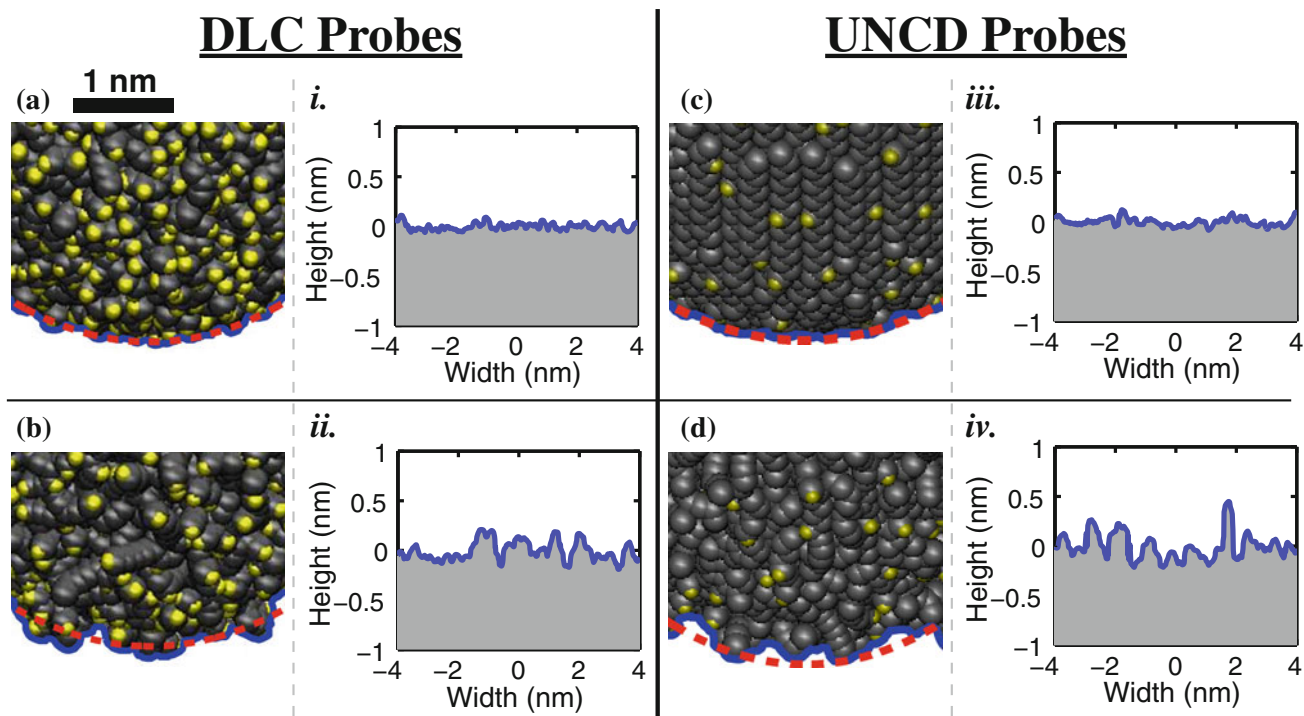


Fig. 3 The roughness of each MD probe shown in Fig. 2 is characterized using side-view renderings (a–d). The outer profiles are traced (blue) and fit to a parabola (red). While the entire profile of the tip was traced and analyzed (approximately 8 nm in arc length), these images of the tip traces have been expanded to show detail. The

subtraction of the two curves (measured and fit) yields the equivalent roughness (shown in i–iv) that would be measured on a flat surface. The original parabolic tips of DLC (a) and UNCD (c) are significantly smoother than the intentionally roughened versions of the same tips (b, d) (Color figure online)

characterizing roughness that could be applied to all tips. Using a high-magnification side-view of the tip, the outermost contours of the profile were traced using a point-selection routine in MATLAB, as shown in Fig. 3a–d. The side-view is created by a rendering program (VMD [40]), where each atom is drawn as a sphere with its corresponding van der Waals radius. Then, after fitting a parabola to the overall traced contour, each traced point was characterized by the magnitude of its distance away from that best-fit parabola. Intuitively, this can be understood as subtracting the overall (parabolic) shape from the actual shape to yield a roughness profile similar to what would be measured on a flat surface (Fig 3i–iv). Once this equivalent profile was obtained, typical roughness characterizations could be performed on it, including the calculation of an RMS roughness value R_q . It should be noted that RMS roughness is ideally measured over a constant sampling area. Unfortunately due to deviations in tip size (especially between the computationally limited MD probes and the coated TEM probes), different sampling widths were unavoidable. While this will add some degree of uncertainty, the increasing roughness of the tips demonstrated by changes in the RMS roughness can clearly be verified by visual inspection of the profiles shown in Figs 3i–iv and 6i–vi.

3.3 Results of Contact Simulations

A video of a typical MD adhesion test is provided in the Supplemental Materials. Pull-off forces and the measured RMS roughness of the simulated MD tips are shown in Table 1. Only data for the approach portion of the curve was analyzed, but in all cases, the approach and retract portions were symmetric and post-test examination showed no

chemical bond formation. For all MD tips (shown in Fig. 2), Eq. 1 and the method described in the introduction was used to calculate the effective work of adhesion. To account for variations in registry of the surface atoms, each tip was tested in five different in-plane positions with respect to the lattice of the diamond surface. The average of the measured values was reported as $F_{\text{pull-off}}$, with the standard deviation of the measurements as the uncertainty in that value. The trends in the data show that as the RMS roughness of the tips increases, the effective work of adhesion decreases. The calculated values for effective work of adhesion of the atomically smooth tips (0.138 J/m^2 and 0.265 J/m^2 , for DLC and UNCD, respectively) are larger than those measured in other recent reports [41, 42], although environments were different (e.g. vacuum vs dry air) and atomic-scale tip roughness values were not measured in those studies.

4 Experimental Adhesion Tests using In Situ TEM

4.1 Experimental Details

Pull-off force measurements were performed inside a TEM (JEOL 2010F with field-emission source) equipped with an in situ indenter (PicoIndenter PI-95, Hysitron, Minneapolis, MN). Silicon AFM chips (PPP-CONT, Nanosensors, Neuchatel, Switzerland) were coated with either 20 nm of DLC by a plasma immersion ion deposition technique (as described in [43]) or with 100 nm of UNCD using hot-filament chemical vapor deposition (as described in [44]). Three DLC AFM probes were tested with experimentally calibrated [45] spring constants of 0.16, 0.30, and 0.36 N/m and tip radii as reported in Table 1. Three UNCD

Table 1 All data from the MD and TEM adhesion tests

Tip material	Sample	Method	Tip radius (nm)	Adhesion force (nN)	RMS roughness (nm)	Eff. work of adhesion (J/m^2)
<i>DLC probes</i>						
DLC (Fig. 2a)	Diamond(111)-H	MD	2.33	2.02 ± 0.10	0.033	0.138 ± 0.007
DLC (Fig. 2b)	Diamond(111)-H	MD	2.67	1.08 ± 0.24	0.098	0.064 ± 0.014
DLC (Fig 5a)	Diamond punch	TEM	45.72	17.1 ± 6.9	0.182	0.060 ± 0.024
DLC (Fig 5b)	Diamond punch	TEM	21.55	1.0 ± 0.4	0.456	0.007 ± 0.003
DLC (Fig 5c)	Diamond punch	TEM	17.40	1.1 ± 0.4	0.548	0.010 ± 0.004
<i>UNCD probes</i>						
UNCD (Fig. 2c)	Diamond(111)-H	MD	2.74	4.56 ± 0.33	0.031	0.265 ± 0.019
UNCD (Fig. 2d)	Diamond(111)-H	MD	2.56	2.02 ± 0.08	0.121	0.125 ± 0.005
UNCD (Fig 5d)	Diamond punch	TEM	37.83	2.1 ± 0.6	0.514	0.009 ± 0.003
UNCD (Fig 5e)	Diamond punch	TEM	70.23	2.6 ± 0.9	0.644	0.006 ± 0.002
UNCD (Fig 5f)	Diamond punch	TEM	115.51	3.2 ± 1.4	1.576	0.004 ± 0.002

For each tip/sample combination, the tip radius is extracted using a parabolic fit to the measured profile and the pull-off force is measured directly. From these values, the effective work of adhesion is calculated using Eq. 1. The RMS roughness is extracted as described in Sect. 3

AFM probes were tested with spring constants of 0.068, 0.12, and 0.16 N/m. The body of the AFM chip was rigidly mounted into the indentation apparatus, opposite a nominally flat, displacement-controlled diamond punch indenter as shown in Fig. 4. Before each set of pull-off tests, the diamond punch was cleaned with light mechanical abrasion and 15 min of ultrasonication in each of three organic solvents. This was followed by a 5-min oxygen/hydrogen treatment in a plasma cleaner (Solarus 950, Gatan, Inc., Pleasanton, CA) to remove surface contamination. In cases where contamination was persistent and not removed by these steps, a focused ion beam was used to remove surface material (tens of nm of depth). Care was taken to minimize beam damage to the remaining diamond surface material (i.e., using a high incidence angle for the cut, and repeating the procedure with decreasing beam current to reduce the damage induced by the previous cut.) Once in the TEM, the diamond punch was brought into contact with the AFM probe, then pulled away at a velocity of approximately 1 nm/s. The adhesion tests were recorded using a video-rate camera (at approximately 30 frames per second). The elastic deflection, Δ , of the cantilever at pull-off was measured in the TEM and multiplied by the spring constant of the cantilever, k_{lever} , to calculate the pull-off force ($F_{\text{pull-off}} = k_{\text{lever}} \cdot \Delta$). The shapes of the probes used in the TEM experiments are shown in Fig. 5a–f. The roughness of each probe was characterized by the method described in Sect. 3 with high resolution still images taken immediately before the adhesion test was performed. The images, traced profiles, and equivalent roughness surfaces of the experimental tips are shown in Fig. 6. Post-test images were also collected to ensure that the tip surface was unchanged. After all testing was performed, the diamond punch was characterized using an AFM (MFP-3D, Asylum Research, Santa Barbara, CA); the RMS roughness was 0.091 nm, as measured over several $100 \times 100 \text{ nm}^2$ areas.

4.2 Results of Experimental Adhesion Tests

A video of a typical in situ TEM adhesion test is provided in the Supplemental Materials. The results for all pull-off tests and roughness characterization of the in situ TEM tests are summarized in Table 1. At least nine adhesion tests were performed on each probe; histograms are provided in Fig. 5i–vi. The average of the measured values was reported as $F_{\text{pull-off}}$ with the standard deviation of the measurements as the uncertainty in that value. There is significant scatter in the data, consistent with results from prior investigations (such as [16]). This scatter is generally attributed to slight changes in alignment [24], which cause registry or disregistry with the atomic corrugation of the opposing surface. The trends in the experimental data are similar to those from the simulation data: the effective work of adhesion for each material shows a strong downward trend with increasing roughness.

5 Comparison of Simulations, Experimental Data, and Theory

5.1 Analysis of all Adhesion Results

The measured values of work of adhesion for all tests (MD and TEM) are shown as a function of RMS roughness in Fig. 7. The atomically smooth MD tips (RMS roughness $\sim 0.03 \text{ nm}$ for both smooth DLC and UNCD tips) with nearly perfect parabolic profiles approach the limit of smoothness that can be physically realized. Therefore, the work of adhesion determined from Eq. 1 for the contact between these tips and the C(111)-H substrate was considered to correspond to a maximum work of adhesion that is realistically attainable, $W_{\text{adh,max}}$, for the given material pairs (0.138 J/m^2 for DLC on C(111)-H, and 0.265 J/m^2 for UNCD on C(111)-H). Each material showed more than

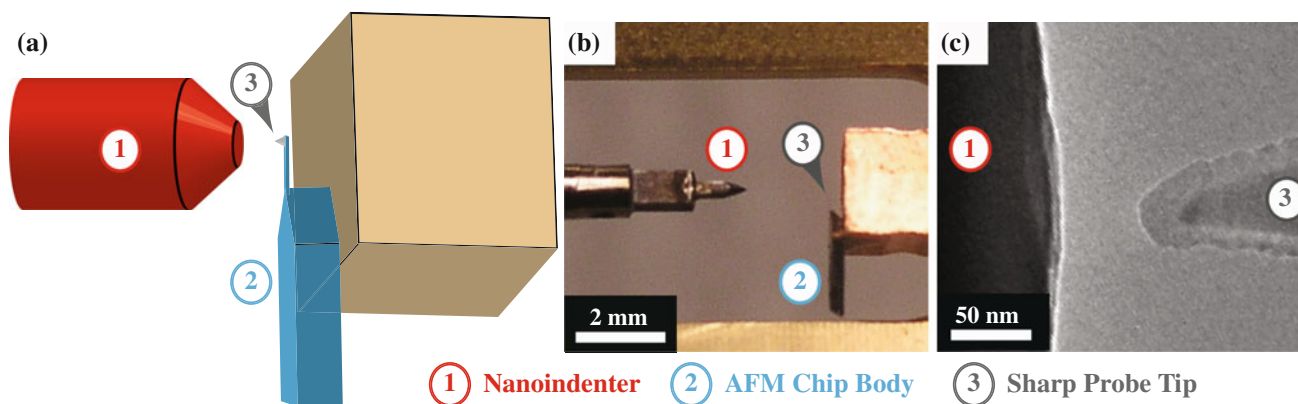


Fig. 4 A schematic representation of the in situ TEM experimental test setup is shown in (a). The actual apparatus is shown using a digital camera (b) and low-resolution TEM imaging (c). The relevant

components are indicated using numbers corresponding to the legend shown below

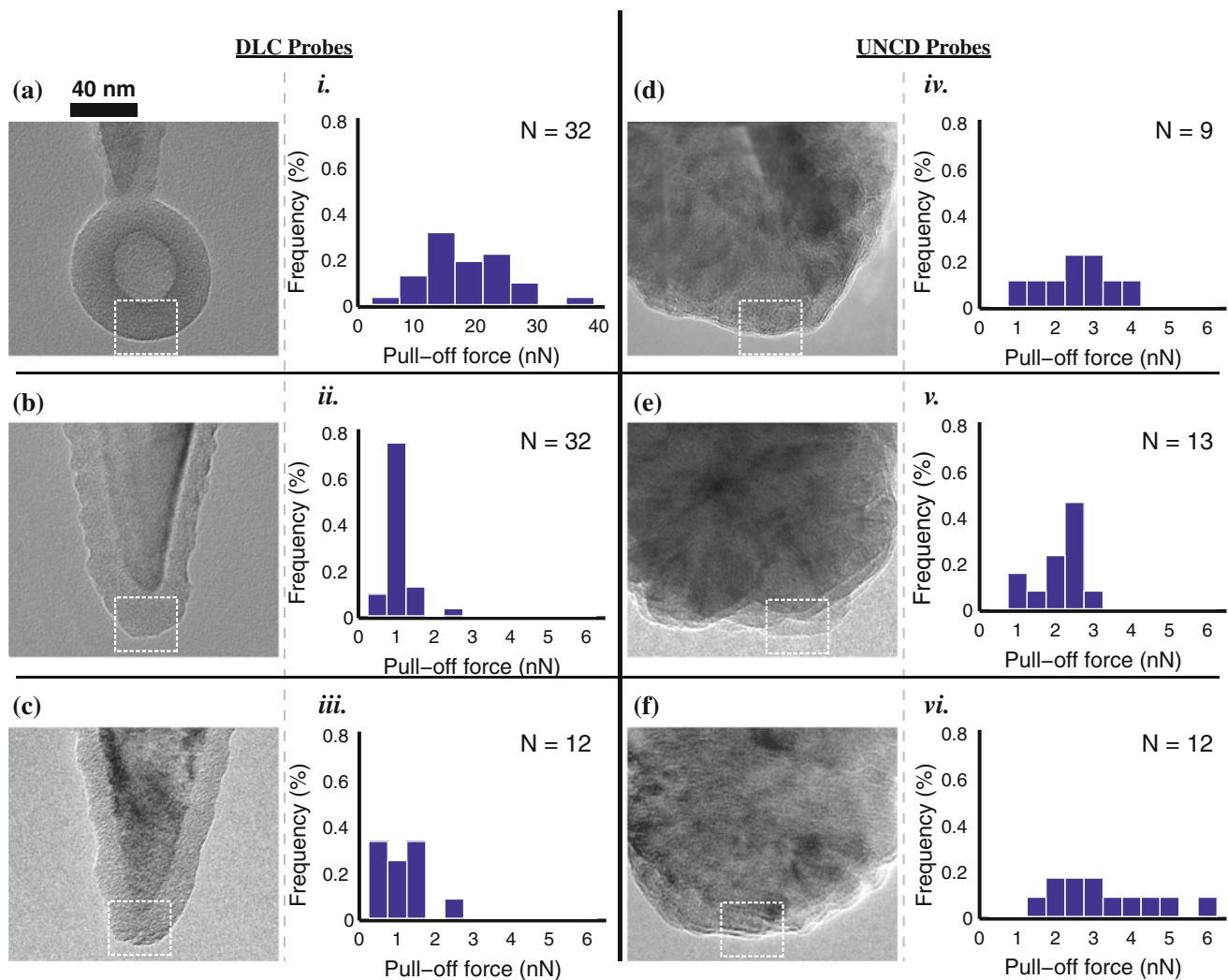


Fig. 5 Three DLC-coated silicon asperities (a–c) and three UNCD-coated silicon asperities (d–f) were used in this study. For the probe shown in (a), an irregularity in the coating process produced an almost perfect hollow sphere on the end of the probe. Each probe was

used for at least 9 pull-off tests; histograms of the measured adhesion force $F_{\text{pull-off}}$ are shown in (i–vi). The *dashed boxes* indicate the regions of the tips that were imaged at higher resolution; the corresponding images are shown in Fig. 6 (Color figure online)

an order of magnitude drop in effective work of adhesion as roughness increased from 0.03 nm (atomically smooth) to approximately 0.5 nm. The magnitude of this decrease in $W_{\text{adh,eff}}$ due to Ångström-level and nanoscale roughness highlights the degree to which measured values of work of adhesion depend on roughness, even when the roughness is at the atomic-scale. The quantity reported in this work as the effective work of adhesion, $W_{\text{adh,eff}}$, represents the value that is commonly reported by applying continuum contact mechanics (Eq. 1) to analyze results from standard probe-based pull-off tests [46]. If the atomic-scale roughness is not measured and explicitly accounted for (which is difficult with nanoscale tips), then the true work of adhesion can be greatly underestimated, and, furthermore, a wide range of values can be measured for the same material pair.

For a given nominal tip radius, there are two sources of variability in the measured adhesion force. The primary effect is the strong decrease in effective work of adhesion among tips of increasing roughness. However, a secondary source of variability arises from differences in the specific contact position, leading to changes in registry and disregistry of the surface corrugations as discussed previously [24]. The results presented here demonstrate that this latter uncertainty shows an increasing trend with roughness (as is clear in Fig. 2i–iv).

One factor that was not considered in the above analysis was the roughness of the (nominally flat) countersurface. However, in all cases, the countersurfaces had a lower RMS roughness than the contacting asperities. In the simulated contacts, the only topographic variations in the hydrogen-terminated (111) face of diamond are due to the

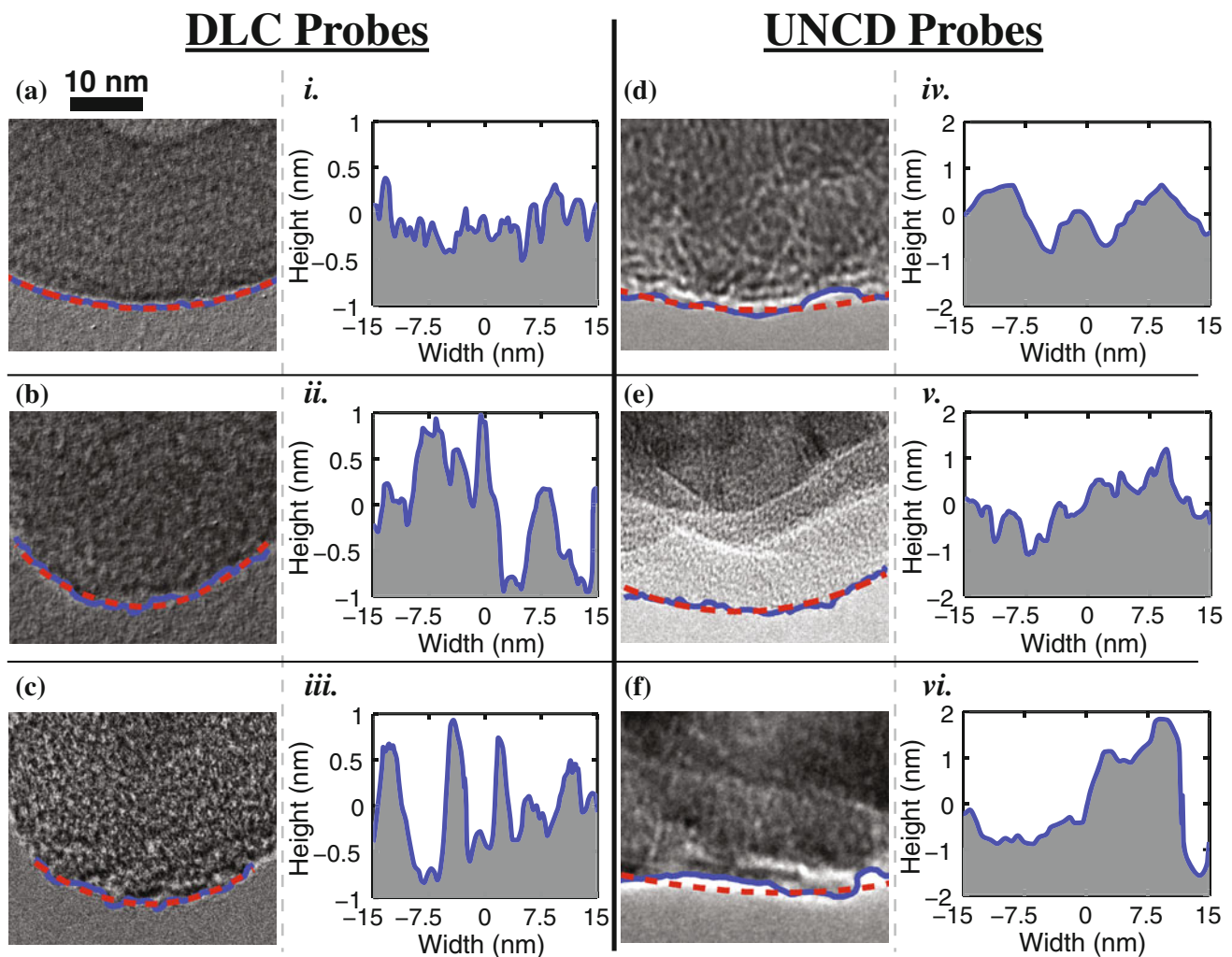


Fig. 6 The roughness of each TEM probe is characterized by the same method that was used for the MD probes (described in Sect. 3). The outer profiles of two-dimensional side views are traced (*blue*) and fit to a parabola (*red*). The subtraction of the two curves yields the equivalent roughness that would be measured on a flat surface; these

profiles are shown in (*i–vi*). For ease of direct visual comparison, the axes of (*i–vi*) have been standardized among the various tips of a single material; in some cases, the profile that was measured and analyzed extends beyond the representative region shown (Color figure online)

atomic corrugation. Thus, these surfaces can be considered to be ideally smooth. In the experimental contacts, the diamond punch appears smooth in the TEM (as shown in Fig. 4c), and ex situ measurements after testing showed an RMS roughness of 0.091 nm, as measured over several $100 \times 100 \text{ nm}^2$ areas. This is not as smooth as the simulated surface, but the roughness is still far lower than that of any of the experimentally measured tips. Therefore, in all cases, the roughness of the substrate is predicted to have only a secondary effect on adhesion.

5.2 Comparison to Model Predictions

To put these results in context, they were compared to predictions from all models discussed in Sect. 1, even though these contacts explicitly violate assumptions made

by many of these models (for example, the assumption that asperity radii R_{asperity} are identical [15, 17, 18, 21]). Note that the self-affine fractal model [19] was not tested because power spectral densities calculated based solely on the two-dimensional profiles seemed insufficient for that purpose. The most readily applicable models are those in which a sphere (radius R_{tip}) in contact with a rough surface is approximated by the same sphere in contact with a single small asperity (radius $r_{\text{model-roughness}}$) situated on a perfectly smooth surface (as pictured in Fig. 1 of [21]). In the latter configuration, the attractive force between the surfaces can be derived analytically by assuming van der Waals adhesion [1, 20]. There are multiple approaches discussed in [15, 21] for determining how the real roughness of a surface should be distilled into the single parameter $r_{\text{model-roughness}}$. The simplest of these approaches is the

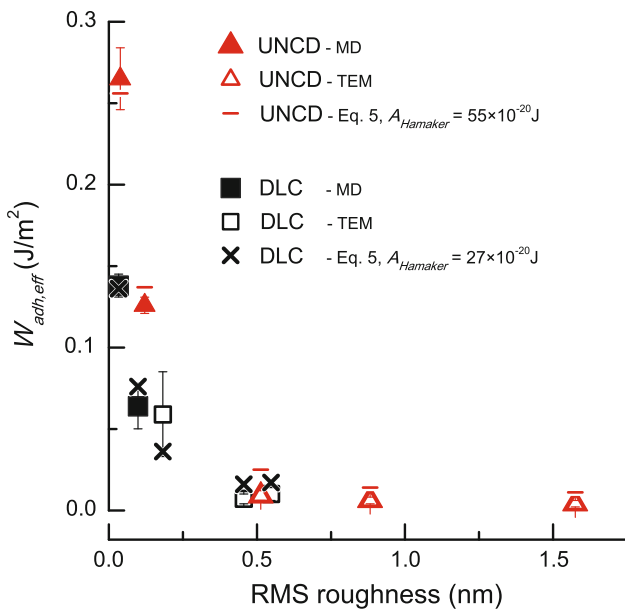


Fig. 7 The work of adhesion decreases by more than an order of magnitude as roughness increases from the sub-Ångström level (atomic corrugation only) to the nanometer-scale. Results from MD simulations (filled data points) and from experimental testing (hollow data points) are shown for sharp tips made of UNCD (red) and of DLC (black). The modified Rumpf model (Eq. 5) was fit separately to each material (indicated by ‘-’s and ‘x’s of corresponding color); the best-fit values of Hamaker constant (designated here $A_{Hamaker}$, for clarity) for each material from fitting the model are given in the legend. The model fits the TEM and MD extremely well (adjusted $R^2 > 0.92$ for both), and the fitting yields physically realistic values for $A_{Hamaker}$ (Color figure online)

modified Rumpf model (discussed in [21]), in which the full roughness is approximated by a single hemispherical asperity on a flat surface, where $r_{model-roughness}$ depends only on the RMS roughness R_q of the surface. Therefore, in this model, the final prediction for pull-off force depends only on R_q (Eq. 7 of [21]). That equation can be combined with Eq. 1 (assuming $\chi = 2$, based on calculated Maugis parameters [4, 9] in the range of 0.012 to 0.108 for the present tests) to predict the effective work of adhesion as follows:

$$W_{adh,eff} = \frac{A_H}{12\pi z_0^2} \left[\left(1 + \frac{R_{tip}}{1.48R_q}\right)^{-1} + \left(1 + \frac{1.48R_q}{z_0}\right)^{-2} \right], \tag{5}$$

where A_H is the Hamaker constant between the two materials.

The present data have been fit using the modified Rumpf model. The input parameters were: the measured pull-off force $F_{pull-off}$; the asperity radii R_{tip} extracted from parabolic fits; and the RMS roughness R_q extracted from the flattened profiles (as described in Sect. 3). The value of z_0 was estimated to be 0.19 nm by the method described in [29] and using the value of the interatomic equilibrium distance taken from the

AIREBO potential. The data for the DLC and UNCD tips were fit separately, each with the Hamaker constant as the only free parameter. Each set of data, which includes measurements from MD and TEM, was well-fit by the model with adjusted R^2 values of 0.927 and 0.989 for DLC and UNCD, respectively. The values for the Hamaker constant extracted from the fits were $A_{H\ DLC:Diamond} = 27 \times 10^{-20}$ J and $A_{H\ UNCD:Diamond} = 55 \times 10^{-20}$ J. These values depend on the choice of z_0 . While specific reference values for these material pairs do not exist, the order of magnitude of these values compares favorably against the reference value of $A_H = 30 \times 10^{-20}$ J calculated for diamond surfaces in a vacuum [1].

Because the modified Rumpf model fits the data well, Eq. 5 can be used to suggest an equation for extracting the smooth-tip work of adhesion, $W_{adh,max}$, from measurements of the effective work of adhesion, $W_{adh,eff}$, if the tip radius and roughness are known. As was done previously, $W_{adh,max}$ is taken as the value that would be measured with a tip containing atomic corrugation ($R_q = 0.03$ nm). In other words, from Eq. 5, $W_{adh,max} = W_{adh,eff}(R_q = 0.03$ nm) and $W_{adh,measured} = W_{adh,eff}(R_q = R_{q,measured})$. These two quantities can be divided, resulting in the following equation:

$$W_{adh,max} = \left[\frac{F_{pull-off}}{2\pi R_{tip}} \right] \frac{\left(1 + \frac{R_{tip}}{1.48(0.03\text{ nm})}\right)^{-1} + \left(1 + \frac{1.48(0.03\text{ nm})}{z_0}\right)^{-2}}{\left(1 + \frac{R_{tip}}{1.48R_q}\right)^{-1} + \left(1 + \frac{1.48R_q}{z_0}\right)^{-2}}. \tag{6}$$

In principle, this is a general equation which allows for the calculation of the work of adhesion that would be measured using an atomically smooth tip (i.e., $W_{adh,max}$). This value should be a fundamental property of the tip-sample interface and should be independent of probe roughness. For instance, in the present study, $W_{adh,max}$ was measured as 0.138 and 0.265 J/m² (DLC and UNCD, respectively) using the atomically smooth simulated tips, but in principle, these values could have been calculated from measurements taken with tips that have finite roughness. In practice, values of $W_{adh,max}$ calculated from the present data agree within 50 % of values measured using the atomically smooth MD tips, but with a high degree of scatter. The scatter is attributed to the relatively small number of measurements. Further work is required to verify the reliability of this approach and the limits of its applicability.

The good agreement of the experimental and simulation data with a simple analytical model holds promise for addressing the challenge of extracting meaningful work of adhesion values from AFM measurements. In general, it is not feasible to characterize the details of the subnanometer-scale roughness of a tip every time a pull-off test is

performed. However, the present results indicate that a reasonable estimate can be made of the effect on work of adhesion with knowledge only of the radius and RMS roughness of the tip material. If a set of tips are fabricated by the same method, TEM characterization of the roughness of a small set could be used to obtain a representative value of RMS roughness R_q , which can then be used with Eq. 6 to extract the smooth-tip work of adhesion.

Regardless of the details of the chosen fitting parameters, Fig. 7 clearly demonstrates several characteristics of the data and the model fit, which can be compared to those of the simplified rigid model presented in Sect. 2:

1. Results show a significant and rapid decrease in the effective work of adhesion with increasing roughness. The TEM and MD results show that for an RMS roughness of just 0.15 nm, the effective work of adhesion is already reduced by approximately 50 % from its smooth-tip value. This trend compares very favorably to the rigid model shown in Fig. 1d, where the same ~ 50 % decrease was observed for an RMS roughness of 0.1 nm
2. The trend of adhesion as a function of roughness not only agrees qualitatively with findings of published models (as demonstrated in Sect. 2) but also can be fit quantitatively using the modified Rumpf model
3. Finally, it may seem surprising that the modified Rumpf model fits well, especially given that it depends only on RMS roughness and does not take into account the spatial extent of the roughness. However, this finding is in agreement with the trend of the simplified rigid model, which showed almost no dependence of $W_{\text{adh,eff}}$ on the wavelength λ . The absence of dependence on wavelength is, in part, because the elastic deformation is very small in these contacts due to the high modulus and relatively low values of adhesion

It is important to note that the power spectral densities (not shown) of both the MD and AFM tips show multiscale roughness, but discussion of the results in terms of such a model is beyond the scope of the present paper.

6 Summary/Conclusions

For the first time, the effect of nanometer- and subnanometer-scale roughness on adhesion of single-asperity contacts has been explored using MD simulation and in situ TEM. Ten asperities (radii of 2–115 nm) of UNCD and DLC have been tested on flat diamond surfaces. The tips had RMS roughness values (calculated as RMS deviation from a smooth analytical parabola fitted to the overall shape of the tip) ranging from 0.03 nm (atomic corrugation only) to 1.58 nm.

Adhesion is shown to be extremely sensitive to atomic-scale roughness in this range. Specifically, work of adhesion values calculated by continuum contact mechanics (which ignore roughness) decreased monotonically from 0.138 and 0.265 J/m² (DLC and UNCD probes, respectively) for atomically smooth tips, down to approximately 0.010 J/m² for the roughest tips of both materials.

The modified Rumpf model is demonstrated to fit the data in Fig. 7 well (adjusted $R^2 = 0.927$ and 0.989 for DLC and UNCD, respectively) and yield reasonable values for the Hamaker constant, which is used as a fit parameter. Therefore, a method is suggested for calculation of a roughness-independent work of adhesion.

Overall, this work highlights the importance of considering atomic-scale roughness when interpreting adhesion specifically and nanoscale contact phenomena more generally. This builds consistently on general points made in previous studies [23, 24] and motivates further studies to understand these phenomena in more detail, as well as further development of practical and reliable strategies for interpreting measurements in AFM where determining the detailed atomic structure of the tip is a challenge.

Acknowledgments The authors wish to thank Dr. Doug Yates and Dr. Ryan Major for microscopy and equipment assistance, and Prof. Mark O. Robbins for helpful discussions. The authors thank Graham E. Wabiszewski for assistance performing AFM on the indenter tip. Use of the facilities of the Pennsylvania Regional Nanotechnology Facility is acknowledged. The authors acknowledge funding from the National Science Foundation under the following Grants: CMMI 0826076 (RWC); IGERT DGE 0221664 (TDBJ); DMR 1120901 (RWC); CMMI 0845294 (KTT); CMMI 0825981 (JAH, PLK, KER); CMMI 1200019 (KTT, RWC); CMMI 1200011 (JAH); and IAA 1129629 (JAH, PLK, KER). KER and PLK also acknowledge partial support from the Office of Naval Research through the US Naval Academy. The support of AFOSR under Contract No. FA2386-11-1-4105 AOARD is also acknowledged (RWC).

References

1. Israelachvili, J.N.: Intermolecular and Surface Forces, 3rd edn. Elsevier, San Francisco (2010)
2. Derjaguin, B.V., Muller, V., Toporov, Y.P.: Effect of contact deformations on the adhesion of particles. *J. Colloid Interface Sci.* **53**, 314–326 (1975)
3. Johnson, K.L., Kendall, K., Roberts, A.D.: Surface energy and the contact of elastic solids. *Proc. R. Soc. Lond. A* **324**, 301–313 (1971)
4. Maugis, D.: Adhesion of spheres: the JKR-DMT transition using a Dugdale model. *J. Colloid Interface Sci.* **150**, 243–269 (1992)
5. Volinsky, A.A., Moody, N.R., Gerberich, W.W.: Interfacial toughness measurements for thin films on substrates. *Acta Mater.* **50**, 441–466 (2002)
6. Gao, H., Wang, X., Yao, H., Gorb, S., et al.: Mechanics of hierarchical adhesion structures of geckos. *Mech. Mater.* **37**, 275–285 (2005)
7. Finnis, M.W.: The theory of metal-ceramic interfaces. *J. Phys. Condens. Matter* **8**, 5811 (1999)

8. Maboudian, R.: Critical review: adhesion in surface micromechanical structures. *J. Vac. Sci. Technol. B* **15**, 1 (1997)
9. Grierson, D., Flater, E., Carpick, R.: Accounting for the JKR–DMT transition in adhesion and friction measurements with atomic force microscopy. *J. Adhes. Sci. Technol.* **19**, 291–311 (2005)
10. Fuller, K., Tabor, D.: Effect of surface-roughness on adhesion of elastic solids. *Proc. R. Soc. Lond. A* **345**, 327–342 (1975)
11. DelRio, F.W., de Boer, M.P., Knapp, J.A., Reedy, E.D., et al.: The role of van der Waals forces in adhesion of micromachined surfaces. *Nat. Mater.* **4**, 629–634 (2005)
12. Tayebi, N., Polycarpou, A.A.: Reducing the effects of adhesion and friction in microelectromechanical systems (MEMS) through surface roughening: comparison between theory and experiments. *J. Appl. Phys.* **98**, 073528 (2005)
13. Ramakrishna, S.N., Clasohm, L.Y., Rao, A., Spencer, N.D.: Controlling adhesion force by means of nanoscale surface roughness. *Langmuir* **27**, 9972–9978 (2011)
14. Segeren, L., Siebum, B., Karszenberg, F.G., Van den Berg, J., et al.: Microparticle adhesion studies by atomic force microscopy. *J. Adhes. Sci. Technol.* **16**, 793–828 (2002)
15. Katainen, J., Paajanen, M., Ahtola, E., Pore, V., et al.: Adhesion as an interplay between particle size and surface roughness. *J. Colloid Interface Sci.* **304**, 524–529 (2006)
16. Liu, D.L., Martin, J., Burnham, N.A.: Which fractal parameter contributes most to adhesion? *J. Adhes. Sci. Technol.* **24**, 2383–2396 (2010)
17. Greenwood, J., Williamson, J.: Contact of nominally flat surfaces. *Proc. R. Soc. Lond. A* **295**, 300–319 (1966)
18. Maugis, D.: On the contact and adhesion of rough surfaces. *J. Adhes. Sci. Technol.* **10**, 161–175 (1996)
19. Peressadko, A., Hosoda, N., Persson, B.: Influence of surface roughness on adhesion between elastic bodies. *Phys. Rev. Lett.* **95**, 124301 (2005)
20. Rumpf, H.: *Particle Technology*. Chapman and Hall, London (1990)
21. Rabinovich, Y.: Adhesion between nanoscale rough surfaces I. Role of asperity geometry. *J. Colloid Interface Sci.* **232**, 10–16 (2000)
22. Mulakaluri, N., Persson, B.: Adhesion between elastic solids with randomly rough surfaces: comparison of analytical theory with molecular-dynamics simulations. *Europhys. Lett.* **96**, 66003 (2011)
23. Luan, B., Robbins, M.: Contact of single asperities with varying adhesion: comparing continuum mechanics to atomistic simulations. *Phys. Rev. E* **74**, 026111 (2006)
24. Piotrowski, P.L., Cannara, R.J., Gao, G., Urban, J.J., et al.: Atomistic factors governing adhesion between diamond, amorphous carbon and model diamond nanocomposite surfaces. *J. Adhes. Sci. Technol.* **24**, 2471–2498 (2010)
25. Liu, J., Grierson, D., Moldovan, N., Notbohm, J., et al.: Preventing nanoscale wear of atomic force microscopy tips through the use of monolithic ultrananocrystalline diamond probes. *Small* **6**, 1140–1149 (2010)
26. Goglia, P.R., Berkowitz, J., Hoehn, J., Xidis, A., et al.: Diamond-like carbon applications in high density hard disc recording heads. *Diam. Relat. Mater.* **10**, 271–277 (2001)
27. Krauss, A.R., Auciello, O., Gruen, D.M., Jayatissa, A., et al.: Ultrananocrystalline diamond thin films for MEMS and moving mechanical assembly devices. *Diam. Relat. Mater.* **10**, 1952–1961 (2001)
28. Greenwood, J.: Adhesion of elastic spheres. *Proc. R. Soc. Lond. A* **453**, 1277–1297 (1997)
29. Yu, N., Polycarpou, A.A.: Adhesive contact based on the Lennard–Jones potential: a correction to the value of the equilibrium distance as used in the potential. *J. Colloid Interface Sci.* **278**, 428–435 (2004)
30. Johnson, K.L.: *Contact Mechanics*. Cambridge University Press, London (2011)
31. Adelman, S.A.: Generalized Langevin equation approach for atom/solid-surface scattering: general formulation for classical scattering off harmonic solids. *J. Chem. Phys.* **64**, 2375 (1976)
32. Auciello, O., Birrell, J., Carlisle, J.A., Gerbi, J.E., et al.: Materials science and fabrication processes for a new MEMS technology based on ultrananocrystalline diamond thin films. *J. Phys. Condens. Matter* **16**, R539–R552 (2004)
33. Stuart, S., Tutein, A., Harrison, J.: A reactive potential for hydrocarbons with intermolecular interactions. *J. Chem. Phys.* **112**, 6472–6486 (2000)
34. LAMMPS Molecular Dynamics Simulator. <http://lammps.sandia.gov/>
35. Plimpton, S.: Fast parallel algorithms for short-range molecular dynamics. *J. Comp. Phys.* **117**, 1–19 (1995)
36. Brenner, D.W., Shenderova, O.A., Harrison, J.A., Stuart, S.J., et al.: A second-generation reactive empirical bond order (REBO) potential energy expression for hydrocarbons. *J. Phys. Condens. Matter* **14**, 783–802 (2002)
37. Harrison, J.A., Schall, J.D., Knippenberg, M.T., Gao, G., et al.: Elucidating atomic-scale friction using molecular dynamics and specialized analysis techniques. *J. Phys. Condens. Matter* **20**, 354009 (2008)
38. Mikulski, P.T., Gao, G., Chateaufneuf, G.M., Harrison, J.A.: Contact forces at the sliding interface: mixed versus pure model alkane monolayers. *J. Chem. Phys.* **122**, 024701 (2005)
39. Knippenberg, M., Mikulski, P., Dunlap, B., Harrison, J.: Atomic contributions to friction and load for tip–self-assembled monolayers interactions. *Phys. Rev. B* **78**, 235409 (2008)
40. Humphrey, W., Dalke, A., Schulten, K.: VMD: visual molecular dynamics. *J. Mol. Graph.* **14**, 33–38 (1996)
41. Sumant, A.V., Grierson, D.S., Gerbi, J.E., Carlisle, J.A., et al.: Surface chemistry and bonding configuration of ultrananocrystalline diamond surfaces and their effects on nanotribological properties. *Phys. Rev. B* **76**, 235429 (2007)
42. Liu, J., Grierson, D.S., Sridharan, K., Carpick, R.W., et al.: Assessment of the mechanical integrity of silicon and diamond-like-carbon coated silicon atomic force microscope probes. In: *Proceedings of the SPIE–The International Society for Optical Engineering*, vol. 7767, p. 776708 (2010)
43. Bares, J.A., Sumant, A.V., Grierson, D.S., Carpick, R.W., et al.: Small amplitude reciprocating wear performance of diamond-like carbon films: dependence of film composition and counterface material. *Tribol. Lett.* **27**, 79–88 (2007)
44. Fletcher, P.C., Felts, J.R., Dai, Z., Jacobs, T.D., et al.: Wear-resistant diamond nanoprobe tips with integrated silicon heater for tip-based nanomanufacturing. *Am. Chem. Soc. Nano* **4**, 3338–3344 (2010)
45. Sader, J., Chon, J., Mulvaney, P.: Calibration of rectangular atomic force microscope cantilevers. *Rev. Sci. Instrum.* **70**, 3967–3969 (1999)
46. Szlufarska, I., Chandross, M., Carpick, R.W.: Recent advances in single-asperity nanotribology. *J. Phys. D–Appl. Phys.* **41**, 123001 (2008)